Virtual Screening of Antimalaria Compounds from Sunflower (Helianthus annuus) Against *Plasmodium falciparum* Dihydroorotate Dehydrogenase (PfDHODH) Target

Purwantiningsih Sugita [1,*] (ID) **, Luthfan Irfana** [1] (ID) **, Arif Fahreza Wiriadibrata** [1]

[1]   Department of Chemistry, Faculty of Mathematics and Natural Sciences, IPB University, Bogor 16680, Indonesia
*   Correspondence: purwantiningsih@apps.ipb.ac.id (P.S.);

Abstract: As one of the novel antimalarial targets, the *Plasmodium falciparum* dihydroorotate dehydrogenase (*Pf*DHODH), which catalyzed the production of orotic acids, needs to be inhibited using natural compounds as an alternative. The development of new drugs needs to be predicted through *in silico* methods to save costs and time through computational means. This study aims to perform virtual screening, through molecular docking simulation, of compounds from sunflower (*Helianthus annuus*), in inhibiting the *Pf*DHODH based on predictions of pharmacokinetics and toxicity. We have virtually screened 155 compounds, and the result showed that the flavonoid hispidulin has the best binding pose and energy of -8.03 kcal/mol and was predicted to be a potential antimalarial candidate based on the parameters of affinity energy, binding site likeness to F1T, as well as pharmacokinetic and toxicity prediction. It also showed that strigolactones and flavonoids dominated ligands with the best affinity energy and the benzopyrans class, which showed a similar structure pattern with F1T.

Keywords: *Helianthus annuus*; molecular docking; *Pf*DHODH.

1. Introduction

Malaria is a tropical infectious disease caused by *Plasmodium falciparum*. The infection is transmitted by female *Anopheles* mosquito bites commonly found in Africa and some areas in Asia [1]. According to data from the World Health Organization, 241 million malaria cases occurred in 2020, with a death rate of around 627,000 people; this number increased by 69,000 people compared to 2019 [2]. Several species of the genus *Plasmodium* that can cause malaria are *P. falciparum*, *P. vivax*, *P. ovale*, and *P. malariae*. However, compared to other species, *P. falciparum* has become the deadliest species which can cause sudden symptoms of malaria activity in humans [3].

Over the past few years, the mutation of malaria parasites and their ability to be resistant to current drugs have challenged the treatment of malaria [4,5]. *Plasmodium falciparum* dihydroorotate dehydrogenase (*Pf*DHODH) catalyzes the oxidation of dihydroorotate to orotic acid. This is crucial in the *de novo* pathway that provides the only pyrimidine source for DNA and RNA biosynthesis since *Plasmodium* lacks pyrimidine salvage enzymes [6–8]. Inhibition of *Pf*DHODH can stop pyrimidine synthesis, which leads to the inhibition of *P. falciparum* cell proliferation.

The back-to-nature approach encourages researchers to explore plant compounds to inhibit pyrimidine synthesis by inhibiting the *Pf*DHODH enzyme. Sunflower (*Helianthus annuus*) is a traditional plant reported to have health benefits such as anti-inflammatory, antipyretic, cathartic, expectorant, stimulant, vermifuge, and antimalarial [9]. It contains secondary metabolic compounds such as alkaloids, phytosterols, steroids, saponins, tannins, and flavonoids. It has been reported that extracts of sunflower parts such as seeds, leaves, roots, flowers, and stalks show good antimalarial activity in both *in vitro* and *in vivo* assays [10–12].

Currently, a new strategy is needed for finding drugs from active compounds in plants efficiently and without high costs. In addition, there are still few studies related to secondary metabolites in *H. annuus,* which are responsible for its antimalarial activity both *in vitro* and *in vivo*. Therefore, *in silico* method can be used to be the first step in the search for candidate drug compounds due to its possibility to tighten the research focus from the produced data, thus saving research costs and can be evaluated for *in vitro* and *in vivo* assays. It has been reported that molecular docking of flavonoid compounds such as catechins, quercetin, luteolin, isoramnetin, kaempferol, fecithin, and myricetin against the *Pf*DHODH enzyme (PDB ID 6GJG) produced a better binding score than standard chloroquine [13]. It is also reported triazolopyrimidine derivatives have good antimalarial activity against the *Pf*DHODH enzyme [8].

One of the most widely used *in silico* methods is molecular docking. It is a powerful approach to understanding drug interactions, design, and discovery. This strategy increases the efficiency of searching for new drugs through computational simulation and calculation by studying molecular behavior through the interaction of bonds between active plant components and receptors [14,15]. This study aims to simulate a virtual screening using molecular docking techniques for *H. annuus* as a *Pf*DHODH enzyme inhibitor and an oral malaria drug candidate based on predictions of pharmacokinetics, toxicity, and similarity to oral drug prediction.

2. Materials and Methods

2.1. Ligand library preparation.

A total of 155 compounds from *H. annuus* were downloaded based on article data from the Knapsack Family (http://www.knapsackfamily.com) and some literature [16–18] using the Simplified Molecular Input Line Entry System (SMILES) notation code. All compound data collected hereinafter referred to as the ligand library (Table S1). The ligand library is converted into an optimal three-dimensional (3D) ligand structure using Gypsum-DL [19]. All ligand structures were simplified and converted to .pdbqt extension files using Open Babel [20].

2.2. Co-crystallized ligand and protein receptor preparation.

The *Pf*DHODH protein (PDB ID 6GJG) was downloaded from Research Collaboratory for Structural Bioinformatics Protein Data Bank (https://www.rcsb.org/structure/6GJG) [21]. The receptor protein was selected based on the best resolution, its role in the malaria pyrimidine synthesis pathway, and the presence of the co-crystallized ligand structure. The receptor protein was visualized and prepared using Chimera 1.16. The protein subunit chain that is not used (Chain B) and the water molecule were removed, leaving chain A protein subunit chain, the flavin mononucleotide (FMN) cofactor, and the orotic acid (ORO) substrate as the receptor. The binding site coordinates are then determined based on the co-crystallized ligand position.

2.3. Molecular docking validation.

The hydrogen atom at pH 7.4 and the Gasteiger charge was added. Co-crystallized ligands were re-docked to the receptor to find the best ligand pose by varying the grid box size and the binding site coordinates. The best grid box size is determined based on the position of the co-crystallized ligand before and after it docked, which is expressed by the root mean squared deviation (RMSD) value.

2.4. Virtual screening.

All ligands were docked to the receptor using the idock program [22]. The results consist of total poses produced and the docking score represented as affinity energy in kcal/mol units. Lipinski's rule of five, drug-likeness scores, and toxicity prediction were reviewed together with docking scores to filter the compounds with the best potency in this study using DataWarrior software [23] and the SwissADME website (http://www.swissadme.ch/) [24]. Ligands with antimalarial activity based on in vitro test results were also included in the screening. An in-depth analysis of ligand-receptor interaction with the best docking scores was done using Chimera 1.16 and LigPlot+ [25].

3. Results and Discussion

3.1. Molecular docking validation.

*Pf*DHODH crystal structure that contains F1T as a competitive inhibitor (PDB ID 6GJG) was used as the receptor protein. This mitochondrial enzyme consists of 371 residues with (β/α)-barrel structure that binds between the two N-terminal of α-helix and a barrel domain body. The protein binding site is adjacent to the FMN cofactor and mostly hydrophobic. The crystal structure was determined by X-ray diffraction in 1.99 Å resolution, which describes the stability of the crystal structure [26,27].

Protein preparation obtains the target protein structure without co-crystal ligands, thus creating room for the docking process [28]. The presence of water molecules can interfere with the docking simulation. Therefore, it needs to be removed to reduce errors, and the test ligand can directly interact with the amino acid residues of the protein. Due to software limitations, hydrogen atoms were added at pH 7.4. This is the nearest value to mitochondrial pH conditions, which work under alkaline conditions with a pH of ~8.0 [29].

■ Co-crystallized ligand initial pose
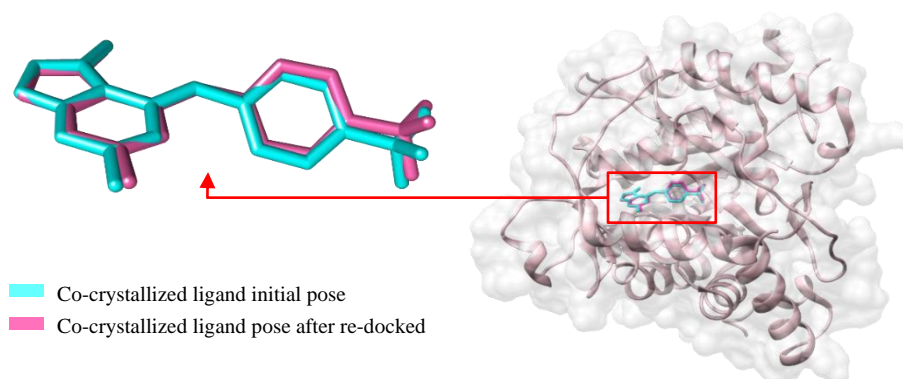■ Co-crystallized ligand pose after re-docked

Figure 1. Molecular docking validation visualization.

The validation result shows the RMSD value of the re-docked co-crystal ligand is 0.385 Å with the affinity energy is -10.12 kcal/mol using a grid box with dimensions $x = 28$, $y = 28$,

and $z = 29$ at coordinates $x = 10.61$, $y = -12.08$, and $z = -4.75$. Figure 1 visualizes the results of the molecular docking validation. It shows that the re-docking simulation reproduces the position of the co-crystallized ligand well because it has a value of <2 Å, which is generally used for successful molecular docking validation criteria [30,31].

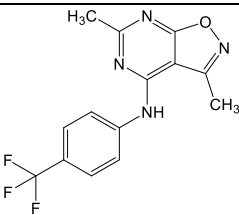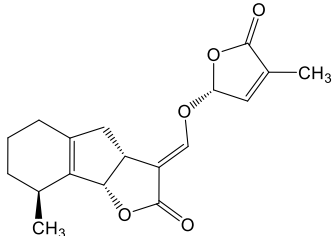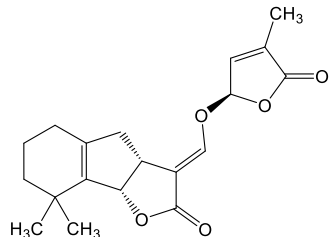### 3.2. Molecular docking and interaction visualization.

The top 10 ligands were selected based on affinity energy, pharmacokinetic properties, and toxicity predictions. Ligands with experimental antimalarial activity were also included. idock program used to quantify affinity energy. Inherited from AutoDock Vina, idock provides a better optimization algorithm and improves the fundamental implementation for more effective virtual screening. It consists of two basic components, including a scoring function to predict affinity energy, which comprises a conformation-dependent and conformation-independent part, and an optimization algorithm to explore the conformational space by attempting to find low-scoring conformations. It uses the Monte Carlo algorithm for global optimization and Broyden-Fletcher-Goldfarb-Shanno (BFGS) Quasi-Newton method for local optimization [8].
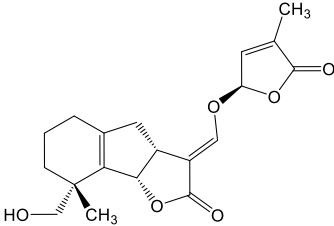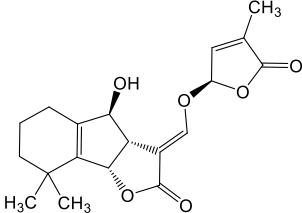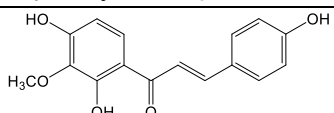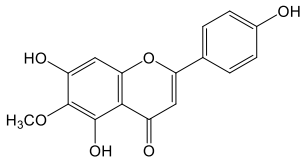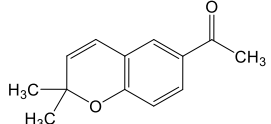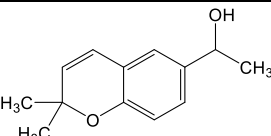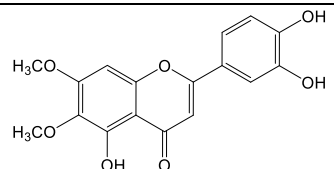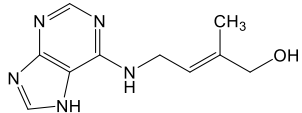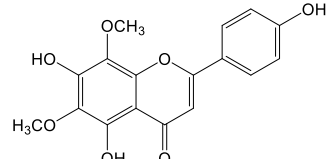
As a result, the top 11 ligands were obtained, which are shown in Table 1. The binding site similarity (BSS) percentage was also calculated based on the ratio between the number of amino acid residues shared by the test and co-crystallized ligands, i.e.:

$$\text{BSS (\%)} = \frac{\Sigma \text{ F1T binding site residue interacting with test ligand}}{\Sigma \text{ F1T binding site residue}} \times 100\%$$

Molecular docking is a methodology applied to study the molecular behavior of target binding, which is carried out by interacting candidate drug compounds (ligands) with protein and analyzing both properties [32].

Table 1. Molecular docking results and binding site similarity calculations.

Compound	Structure	Affinity energy (kcal/mol)	BSS (%)
F1T (Co-crystallized ligand)		-10.12	-
Sorgolactone (1)		-9.31	90.91
5-Deoxystrigol (2)		-9.20	90.91

Compound	Structure	Affinity energy (kcal/mol)	BSS (%)
Sorgomol (3)		-8.34	90.91
Orobanchol (4)		-8.31	81.82
Kukulkanin B (5)		-8.29	81.82
Hispidulin (6)		-8.03	100
Demetoxyiencecalin (7)		-7.73	45.45
Demetoxyencecalinol (8)		-7.63	72.73
Cirsiliol (9)		-7.60	81.82
trans-Zeatin (10)		-7.47	81.82
Demetoxysudachitin (11)		-6.19	0

Affinity energy is described as the change of Gibbs free energy (ΔG), a ligand-receptor bond stability parameter, and represents the energy involved during the binding process. The lower the value, the stronger the ligand-receptor bond and the more spontaneous physical reactions that occur due to the formation of bonds in the ligand-receptor complex due to the release of free energy during the reaction [33].

All test ligands' affinity energy are shown in Table S1. F1T produces the most exergonic affinity energy, -10.12 kcal/mol. Based on the results obtained, the most exergonic affinity energy from the top 11 selected ligands was obtained by ligand (1). On the other side, the

highest BSS percentage was produced by ligand (**6**), whereas the lowest value was produced by ligand (**11**), which also had the least exergonic affinity energy.

Visualization of ligand-receptor interactions was performed in two dimensions (2D) and three dimensions (3D). F1T interact with 11 amino acid residues, two of them, which are Arg265 and His185, form hydrogen bonds with a bond length of 3.05 Å and 3.06 Å, respectively. The other 10 residues formed hydrophobic interactions. F1T inhibits the binding site between FMN and the N-terminal of the α-helix, the binding site for coenzyme Q (CoQ). In the absence of CoQ, the production of orotic acid will not occur. Orotic acid is well-known as a precursor in the biosynthesis of pyrimidines, which are released from the mitochondrial DHODH in mammals. Thus, the absence of orotic acid led to no pyrimidine formation. The enzyme-bound structure indicates that F1T occupies most of the available binding sites, and the presence of the FMN cofactor could potentially accommodate additional functionality [21,34,35].

(**a**)   (**b**)   (**c**)
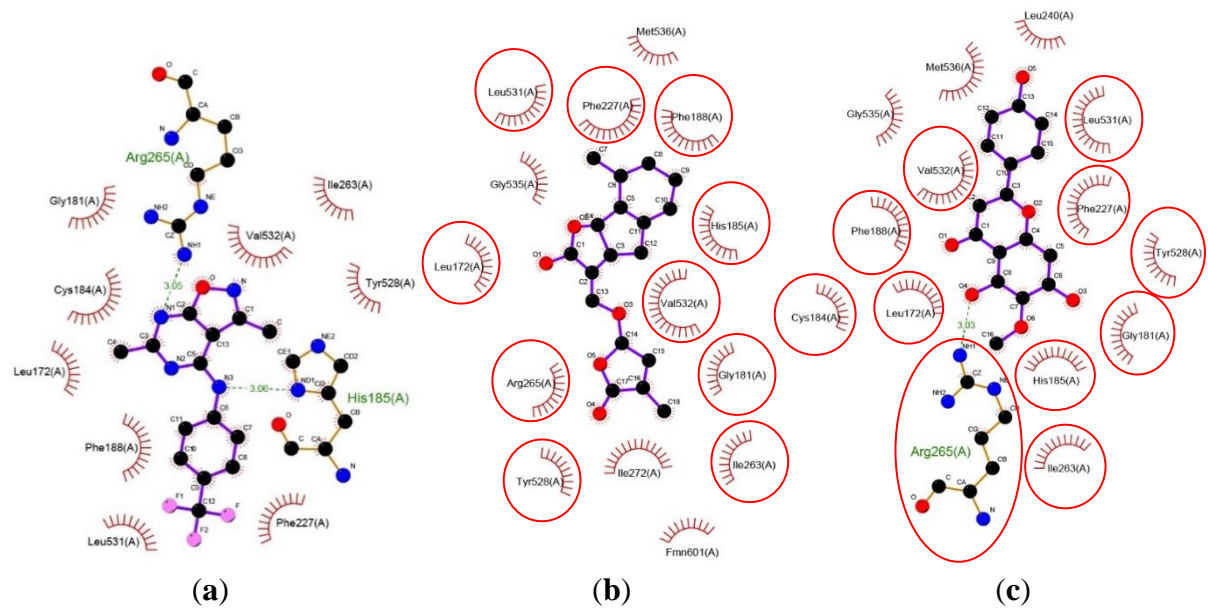
Figure 2. Interaction of F1T (**a**), sorgolactone (**b**), and hispidulin (**c**) ligands with *Pf*DHODH residues in 2D.

(**a**)   (**b**)   (**c**)
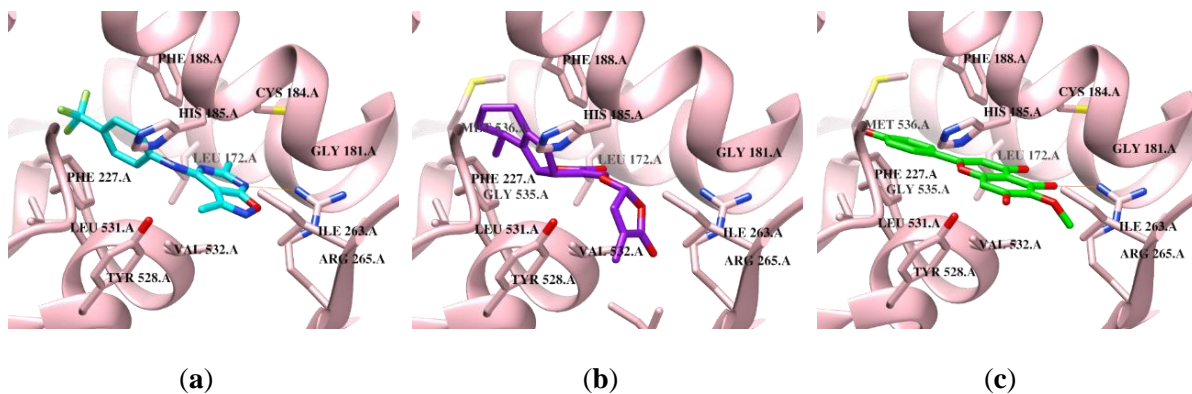
Figure 3. Interaction of F1T (**a**), sorgolactone (**b**), and hispidulin (**c**) ligands with *Pf*DHODH residues in 3D.

Ligand (**1**), which has the most exergonic affinity energy among the 10 other test ligands, shows interactions between amino acid residues quite similar to F1T. It shows the hydrophobic interaction with 14 residues. Whereas ligand (**6**) has the highest BSS percentage, forms a hydrogen bond with Arg265 with a bond length of 3.03 Å, and forms a hydrophobic interaction with 13 residues (Figures 2 and 3).

Amino acid residues difference cause the different affinity energies produced. His185 and Arg265 are two important residues in *Pf*DHODH binding site which contribute to the affinity energy produced [21]. In addition, it is also reported that the π-stacking hydrophobic interaction between Phe227 and Phe188 residues contributed to the resulting affinity energy [35]. In this case, F1T, ligand (**1**), and ligand (**6**) are predicted to bind with the two residues. Hydrophobic interactions between ligands and amino acid residues at *Pf*DHODH binding site tend to have a greater affinity energy effect than hydrogen bonds. This is indicated by the affinity energy of ligand (**1**) being smaller than ligand (**6**). Hydrophobic interactions involve more structural parts of the compound and residues, thus making the interaction zone wider, allowing a more significant pose to changes and affecting ligand binding in the receptor.

On the other side, it is in contrast to the affinity energy of F1T, which does not create hydrophobic interactions with Arg265 and His185. The low-affinity energy occurs due to the presence of the -CF$_3$ group attached to the aromatic ring, which tends to increase the docking activity [8]. The presence of -CF$_3$ groups increases the bioactivity of ligands in proteins and affinity energy, mostly driven by electrostatic energy [36]. The visualization of other test ligand interactions is shown in Figure S1–S3.

3.3. Pharmacokinetic properties and toxicity prediction.

Pharmacokinetic properties and ligands toxicity were predicted computationally using DataWarrior and SwissADME. The pharmacokinetic predictions of the ligands refer to Lipinski's rules of five (RO5), including molecular weight ≤500 Da, partition coefficient of a compound between *n*-octanol and water (LogP) ≤5, hydrogen donors ≤5, hydrogen acceptors ≤10, and molar refractivity values between 40–130. Lipinski's RO5 is based on the properties distribution calculation from several thousand drugs. It describes the properties of orally active compounds based on their pharmacological activity when consumed by humans. It also describes the solubility of certain compounds to permeate to cell membranes through passive diffusion [37–39]. The results are presented in Table 2, which shows that all ligands have met all the criteria in Lipinski's RO5. It is reported that compounds with high potential as oral drugs are the ones with no violate more than two parameters which describes the poor absorptions in the body. Based on the RO5, all ligands can be said to have good solubility in the body as indicated by the fulfillment of RO5.

Table 2. Pharmacokinetic properties of ligands based on Lipinski's RO5.

Compounds	Molecular Weight (Da)	LogP	Hydrogen Acceptors	Hydrogen Donors	Molar Refractivity
F1T (Co-crystallized ligand)	308.26	3.47	5	1	74.08
Sorgolactone (**1**)	316.13	1.72	5	0	82.42
5-Deoxystrigol (**2**)	330.15	2.05	5	0	86.96
Sorgomol (**3**)	346.14	1.13	6	1	88.13
Orobanchol (**4**)	346.14	1.20	6	1	88.13
Kukulkanin B (**5**)	286.28	0.62	5	2	78.81
Hispidulin (**6**)	300.06	-2.47	6	0	80.48
Demetoxyiencecalin (**7**)	202.10	2.56	2	0	60.76
Demetoxyencecalinol (**8**)	204.12	2.38	2	1	61.5
Cirsiliol (**9**)	330.07	-2.54	7	0	86.97
trans-Zeatin (**10**)	219.11	-3.24	6	3	60.91
Demetoxysudachitin (**11**)	330.29	-0.96	7	1	86.97

Toxicity prediction is one of the important steps that must be strictly ensured in drug design before clinical tests are carried out to determine the ability of a compound to cause cell

damage when exposed to organisms [40]. It can be done quantitatively or qualitatively with several determining factors, such as route, frequency and duration of exposure, the dose used, ADME properties, biological properties, and the chemical properties of these compounds [41]. This study uses a qualitative toxicity prediction with parameters such as mutagenic properties, tumorigenic properties, irritation effects, reproductive system effects, and unwanted functional groups.

Based on the results, ligand (**11**) has high-intensity tumorigenic properties (Table 3). It has side effects if consumed by the human body theoretically. Tumorigenic properties are the tendency of a compound to produce tumors. However, despite having toxic effects on the body, ligand (**11**) has the highest drug-likeness score, while the lowest score is obtained by ligand (**3**). Functional group modification is an alternative to changing the compound toxicity profile to obtain a chemical structure that is more effective and safe for the body [42].

Table 3. Toxicity prediction and drug-likeness score

Compound	M [1]	T [2]	RE [3]	I [4]	Unwanted Functional Group			DS [6]
					DataWarrior [23]	Brenk [43]	PAINS [5] [44]	
F1T (Co-crystallized ligand)	-	-	-	-	-	-	-	-6.25
Demetoxysudachitin (**11**)	-	++	-	-	-	-	-	0.45
Hispidulin (**6**)	-	-	-	-	-	-	-	0.40
Cirsiliol (**9**)	-	-	-	-	-	1	1	0.40
Kukulkanin B (**5**)	-	-	-	-	-	1	-	0.26
trans-Zeatin (**10**)	-	-	-	-	-	1	-	-0.84
Sorgolactone (**1**)	-	-	-	-	-	4	-	-1.36
Orobanchol (**4**)	-	-	-	-	-	4	-	-2.51
Demetoxyiencecalin (**7**)	-	-	-	-	-	-	-	-2.60
5-Deoxystrigol (**2**)	-	-	-	-	-	4	-	-2.89
Demetoxyencecalinol (**8**)	-	-	-	-	-	-	-	-3.67
Sorgomol (**3**)	-	-	-	-	-	4	-	-7.94

[1] Mutagenic; [2] Tumorigenic; [3] Reproductive Effects; [4] Irritant; [5] Pan Assay Interference Compounds; [6] Druglikeness Score

The drug-likeness score is defined as the value of a compound's various molecular properties and structures that lead to similarity to commercial drugs. A positive value on the drug-likeness score illustrates that the compound contains most of the common fragments found in commercial drugs to be consumed orally [45]. In this case, 4 compounds that have a positive drug-likeness score, such as ligands (11), (6), (9), and (5), are predicted to be taken orally. A total of 10 ligands had a better drug-likeness score than co-crystallized ligands, including ligands (1), (2), (4), (5), (6), (7), (8), (9), (10), and (11), while ligand (3) had a lower drug-likeness score compared to the co-crystallized ligand.

Despite having the most exergonic affinity energy, the strigolactone ligand (1) showed the presence of unwanted functional groups according to Brenk *et al.*, including the enol group (-C=C-OH), Michael acceptors (-C=C-C=O) which associated with adverse drug reactions [46], and esters (Figure 4). These groups are potentially mutagenic and reactive if consumed. Ligand (2), ligand (3), and ligand (4), which belong to the same compound class as ligand (1), are also predicted to have the same four unwanted functional groups. Besides these four ligands, two ligands with a positive drug-likeness score are predicted to have unwanted functional groups: Ligand (5) contains the Michael acceptor, and ligand (9) contains the catechol ring. Ligand (10) is predicted to have one functional group that needs to be avoided, like isolated alkene. It is necessary to further lead optimization and QSAR studies on the 11 ligands that resulted from this virtual screening against PfDHODH to further assess its potential as antimalarial agents.
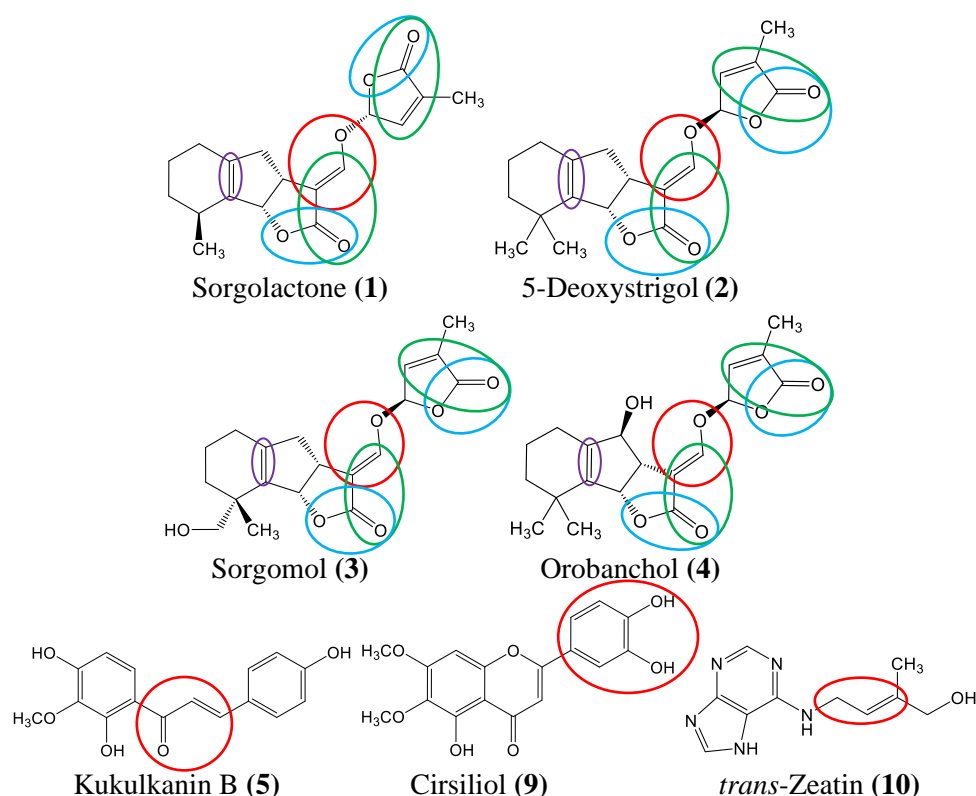
Figure 4. Predicted unwanted functional groups: Enol (red), isolated alkene (purple), Michael acceptor (green), and ester (cyan).

Aside from Brenk's analysis, Pan Assay Interference Compounds (PAINS) analysis was also carried out to determine the reactivity and selectivity of compounds to receptor proteins based on their structure [44]. One unwanted functional group was shown in the ligand (**9**). This group includes a catechol ring due to its possibility to reduce the selectivity of the receptor its reactivity [47]. Ligand (**6**), one of the ligands with the best affinity energy, is predicted to be safe if consumed with no toxic properties, either mutagenic properties, tumorigenic properties, reproductive effects, irritating effects, or the absence of unwanted groups. This compound is predicted to be taken orally due to its positive drug-likeness score.

Although some ligands are predicted to have toxic properties, further experimental research on 11 ligands screened here is needed to assess their potential as antimalarial drug candidates, such as *in vitro* assay to see their biological activity in the culture of living cells [48]. It is also suggested to do further computational research like molecular dynamic or quantum mechanical study to verify the results above due to molecular docking method limitations. In molecular docking, important intermolecular interaction terms, such as solvation effect and entropy change, are highly simplified; thus the scoring function can only give coarse binding energy estimates [49].

4. Conclusions

A total of 11 out of 155 natural product compounds from *H. annuss* were virtually screened based on the prediction of affinity energy to *pf*DHODH by molecular docking, pharmacokinetic properties, toxicity predictions, and their activity as antimalarials based on *in vitro* tests. Hispidulin (**6**), a flavonoid compound, is one of the ligands with the best affinity energy, which is -8.03 kcal/mol, and is predicted to have potential as a candidate for oral antimalarial drugs. This ligand occupies Lipinski's RO5, binds to important amino acid residues, and has no side effects in predicting toxicity such as mutagenic properties,

tumorigenic properties, reproductive effects, irritating effects, absence of unwanted functional groups, and has a good drug-likeness score.

Funding

Acknowledgments

Conflicts of Interest

No conflicts of interest are disclosed by the authors.

References

1. Talapko, J.; Škrlec, I.; Alebić, T.; Jukić, M.; Včev, A. Malaria: the past and the present. *Microorganisms* **2019**, *7*, 1–17, https://doi.org/10.3390/microorganisms7060179.
2. Word Malaria Report 2021. Global Malaria Programme World Health Organization: Geneva, Switzerland, **2021**, ISBN 978-92-4-004049-6, https://www.who.int/teams/global-malaria-programme/reports/world-malaria-report-2021.
3. Sharma, B.; Singh, P.; Singh, A.K.; Awasthi, S.K. Advancement of chimeric hybrid drugs to cure malaria infection: An overview with special emphasis on endoperoxide pharmacophores. *Eur. J. Med. Chem.* **2021**, *219*, 1–37, https://doi.org/10.1016/j.ejmech.2021.113408.
4. Silveira, F.F.; de Souza, J.O.; Hoelz, L.V.B.; Campos, V.R.; Jabor, V.A.P.; Aguiar, A.C.C.; Nonato, M.C.; Albuquerque, M.G.; Guido, R.V.C.; Boechat, N.; Pinheiro, L.C.S. Comparative study between the anti-*P. falciparum* activity of triazolopyrimidine, pyrazolopyrimidine and quinoline derivatives and the identification of new PfDHODH inhibitors. *Eur. J. Med. Chem.* accepted, https://doi.org/10.1016/j.ejmech.2020.112941.
5. Ibrahim, Z.Y.; Uzairu, A.; Shallangwa, G.A.; Abechi, S.E. Pharmacokinetic predictions and docking studies of substituted aryl amine-based triazolopyrimidine designed inhibitors of *Plasmodium falciparum* dihydroorotate dehydrogenase (*Pf*DHODH). *Futur. J. Pharm. Sci.* **2021**, *7*, 1–10, https://doi.org/10.1186/s43094-021-00288-2.
6. Phillips, M.A.; Rathod, P.K. *Plasmodium* dihydroorotate dehydrogenase: a promising target for novel antimalarial chemotherapy. *Infect. Disord. Drug Targets* **2010**, *10*, 226–239, https://doi.org/10.2174/187152610791163336.
7. Coteron. J.M.; Marco, M.; Esquivias, J.; Deng, X.; White, K.L.; White, J.; Koltun, M.; Mazouni, F.E.; Kokkonda, S.; Katneni, K. *et al*. Structure-guided lead optimization of triazolopyrimidine-ring substituents identifies potent *Plasmodium falciparum* dihydroorotate dehydrogenase inhibitors with clinical candidate potential. *J. Med. Chem.* **2011**, *54*, 5540–5561, https://doi.org/10.1021/jm200592f.
8. Hoelz, L.V.; Calil, F.A.; Nonato, M.C.; Pinheiro, L.C.; Boechat, N. *Plasmodium falciparum* dihydroorotate dehydrogenase: a drug target against malaria. *Future Med. Chem.* **2018**, *10*, 1853–1874 https://doi.org/10.4155/fmc-2017-0250.
9. Laksemi, D.A.A.S.; Sukrama, I.D.M.; Suwanti, L.T.; Sudarmaja, I.M.; Damayanti, P.A.A.; Tunas, I.K. A comprehensive review on medicinal plants potentially as antimalarial. *Trop. J. Nat. Prod. Res.* **2022**, *6*, 287–298, https://doi.org/10.26538/tjnpr/v6i3.1 .
10. Ekasari, W.; Pratiwi, D.W.; Amanda, Z.; Suciati; Widyawaruyanti, A.; Arwati, H. Various parts of *Helianthus annuus* plants as new sources of antimalarial drugs. *Evidence-Based Complement. Altern. Med.* **2019**, *2019*, 1–7, https://doi.org/10.1155/2019/7390385.
11. Marangoh, N.; Suciati; Ekasari, W. *In vitro* antimalarial activity and toxicity of *Helianthus annuus* L. leaf extract against *Plasmodium falciparum*. *J. Farm. Dan Ilmu Kefarmasian Indones.* **2021**, *8*, 259–263, https://doi.org/10.20473/jfiki.v8i32021.259-263.

12. Ngibad, K. Efektivitas kombinasi ekstrak etanol daun bunga matahari (*Helianthus annuus*) dan tanaman anting-anting (*Acalypha indica* Linn) sebagai antimalaria secara *in vivo*. *J. Farm. Galen.* **2019**, *5*, 12–19, https://doi.org/10.22487/j24428744.2019.v5.i1.11860.

13. Owoloye, A.; Enejoh, O.A.; Akanbi, O.M.; Bankole O.M. Molecular docking analysis of Plasmodium falciparum dihydroorotate dehydrogenase from towards the design of effective inhibitors. *Bioinformation* **2020**, *16*, 672–679, https://doi.org/10.6026/97320630016672.

14. Prieto-Martínez, F.D.; Arciniega, M.; Medina-Franco, J.L. Molecular docking: current advances and challenges. *TIP Rev. Espec. en Ciencias Químico-Biológicas* **2018**, *21*, 65–87, https://doi.org/10.22201/fesz.23958723e.2018.0.143.

15. Morenikeji, O.R.; Poyi, O.C.; Odumosu, P.O.; Agwom, F.M.; Onah, J.O. *In silico* analysis of azadirachtin and its analogs on dihydrofolate reductase of *Plasmodium* species. *Appl. Biol. Chem. J.* **2022**, *3*, 47–55, https://www.theabcjournal.com/index.php/tabcj/article/view/49.

16. Qiao, Z.; Han, L.; Liu, X.; Dai, H.; Liu, C.; Yan, M.; Li, W.; Han, W.; Li, X.; Huang, S. *et al.* Extraction, radical scavenging activities, and chemical composition identification of flavonoids from sunflower (*Helianthus annuus* L.) receptacles. *Molecules* **2021**, *26*, 1–18, https://doi.org/10.3390/molecules26020403.

17. Silva, D.B.; Aschenbrenner, A.K.; Lopes, N.P.; Spring, O. Direct analyses of secondary metabolites by mass spectrometry imaging (MSI) from sunflower (*Helianthus annuus* L.) trichomes. *Molecules* **2017**, *22*, 1–11, https://doi.org/10.3390/molecules22050774.

18. Macías, F.A.; Molinillo, J.M.G.; Torres, A.; Varela, R.M.; Castellano, D. Bioactive flavonoids from *Helianthus annuus* cultivars. *Phytochemistry* **1997**, *45*, 683–687, https://doi.org/10.1016/S0031-9422(97)00011-3.

19. Ropp, P.J.; Spiegel, J.O.; Walker, J.L.; Green, H.; Morales, G.A.; Milliken, K.A.; Ringe, J.J.; Durrant, J.D. Gypsum-DL: an open-source program for preparing small-molecule libraries for structure-based virtual screening. *J. Cheminform.* **2019**, *11*, 1–13, https://doi.org/10.1186/s13321-019-0358-3.

20. O'Boyle, N.M.; Banck, M.; James, C.A.; Morley, C.; Vandermeersch, T.; Hutchison, G.R. Open Babel: an open chemical toolbox. *J. Cheminform.* **2011**, *3*, 1–14, https://doi.org/10.1186/1758-2946-3-33.

21. Kokkonda, S.; Mazouni, F.E.; White, K.L.; White, J.; Shackleford, D.M.; Lafuente-Monasterio, M.J.; Rowland, P.; Manjalanagara, K.; Joseph, J.T.; Garcia-Pérez, A. *et al.* Isoxazolopyrimidine-based inhibitors of *Plasmodium falciparum* dihydroorotate dehydrogenase with antimalarial activity. *ACS Omega* **2018**, *3*, 9227–9240, https://doi.org/10.1021/acsomega.8b01573.

22. Li, H.; Leung, K.S.; Wong, M.H. idock: a multithreaded virtual screening tool for flexible ligand docking. *2012 IEEE Symp. Comput. Intell. Comput. Biol.* **2012**, 77–84, https://doi.org/10.1109/CIBCB.2012.6217214.

23. López-López, E.; Naveja, J.J.; Medina-Franco, J.L. DataWarrior: an evaluation of the open-source drug discovery tool. *Expert Opin. Drug Discov.* **2019**, *14*, 335–341, https://doi.org/10.1080/17460441.2019.1581170.

24. Daina, A.; Michielin, O.; Zoete, V. SwissADME: A free web tool to evaluate pharmacokinetics, drug-likeness and medicinal chemistry friendliness of small molecules. *Sci. Rep.* **2017**, *7*, 1–13, https://doi.org/10.1038/srep42717.

25. Laskowski, R.A.; Swindells, M.B. LigPlot+: multiple ligand-protein interaction diagrams for drug discovery. *J. Chem. Inf. Model.* **2011**, *51*, 2778–2786, https://doi.org/10.1021/ci200227u.

26. Lu, H.M.; Yin, D.C.; Ye, Y.J.; Luo, H.M.; Geng, L.Q.; Li, H.S.; Guo, W.H.; Shang, P. Correlation between protein sequence similarity and x-ray diffraction quality in the Protein Data Bank. *Protein Pept. Lett.* **2009**, *16*, 50–55, https://doi.org/10.2174/092986609787049457.

27. Ferdian, P.R.; Elfirta, R.R.; Ikhwani, A.Z.N.; Kasirah; Haerul; Sutardi, D.; Ruhiat, G. Studi *in silico* senyawa fenolik madu sebagai kandidat inhibitor Mpro SARS-CoV-2. *Media Penelit. dan Pengemb. Kesehat.* **2021**, *31*, 213–232, https://doi.org/10.22435/mpk.v31i3.4920.

28. Adnyani, K.D.; Lestari, L.W.E.; Prabowo, H.; Siaka, P.A.I.A.; Laksmiani, N.P.L. Aktivitas dari kuersetin sebagai agen pencerah kulit secara *in silico*. *J. Kim.* **2019**, *13*, 207–212, https://doi.org/10.24843/jchem.2019.v13.i02.p14.

29. Lin, B.; Wei, Y.; Hao, Y.; Suang, E.; Shu, Y.; Wang, J. β-Naphthothiazolium-based ratiometric fluorescent probe with ideal pKa for pH imaging in mitochondria of living cells. *Talanta* **2021**, *232*, 1–10, https://doi.org/10.1016/j.talanta.2021.122475.

30. Jain, A.N.; Nicholls, A. Recommendations for evaluation of computational methods. *J. Comput. Aided. Mol. Des.* **2008**, *22*, 133–139, https://doi.org/10.1007/s10822-008-9196-5.

31. García-Godoy, M.J.; López-Camacho, E.; García-Nieto, J.; Nebro, A.J.; Aldana-Montes, J.F. Molecular docking optimization in the context of multi-drug resistant and sensitive EGFR mutants. *Molecules* **2016**, *21*, 1–14, https://doi.org/10.3390/molecules21111575.

32. Bare, Y.; Rophi, A.H.; Tiring, S.S.N.D.; Rachmad, Y.T.; Nugraha, F.A.D.; Sari, D.R. prediction potential chlorogenic acid as inhibitor ace (*in silico* study). *Bioscience* **2019**, *3*, 197–203, https://doi.org/10.24036/0201932105856-0-00.

33. Suhadi, A.; Rizarullah, R.; Feriyani, F. Simulasi penambatan senyawa aktif daun binahong sebagai inhibitor enzyme aldose reductase. *Sel J. Penelit. Kesehat.* **2019**, *6*, 55–65, https://doi.org/10.22435/sel.v6i2.1651.

34. Phillips, M.A.; Lotharius, J.; Marsh, K.; White, J.; Dayan, A.; White, K.L.; Njoroge, J.W.; Mazouni, F.E.; Lao, Y.; Kokkonda, S. *et al.* A long-duration dihydroorotate dehydrogenase inhibitor (DSM265) for prevention and treatment of malaria. *Sci. Transl. Med.* **2015**, *7*, 1–12, https://doi.org/10.1126/scitranslmed.aaa6645.

35. Deng, X.; Gujjar, R.; Mazouni, F.E.; Kaminsky, W.; Malmquist, N.A.; Goldsmith, E.J.; Rathod, P.K.; Phillips, M.A. Structural plasticity of malaria dihydroorotate dehydrogenase allows selective binding of diverse chemical scaffolds. *J. Biol. Chem.* **2009**, *284*, 26999–27009, https://doi.org/10.1074/jbc.M109.028589.

36. Abula, A.; Xu, Z.; Zhu, Z.; Peng, C.; Chen, Z.; Zhu, W.; Aisa, H.A. Substitution effect of the trifluoromethyl group on the bioactivity in medicinal chemistry: statistical analysis and energy calculations. *J. Chem. Inf. Model.* **2020**, *60*, 6242–6250, https://doi.org/10.1021/acs.jcim.0c00898.

37. Zubair, M.S.; Maulana, S.; Mukaddas, A. Penambatan molekuler dan simulasi dinamika molekuler senyawa dari genus *Nigella* terhadap penghambatan aktivitas enzim protease HIV-1. *J. Farm. Galen.* **2020**, *6*, 132–140, https://doi.org/10.22487/j24428744.2020.v6.i1.14982.

38. Narkhede, R.R.; Pise, A.V.; Cheke, R.S.; Shinde, S.D. Recognition of natural products as potential inhibitors of COVID-19 main protease (Mpro): *in-silico* evidence. *Nat. Products Bioprospect.* **2020**, *10*, 297–306, https://doi.org/10.1007/s13659-020-00253-1.

39. Kekessie, F.K.; Amengor, C.D.K.; Brobbey, A.; Addotey, J.N.; Danquah, C.A.; Peprah, P.; Harley, B.K.; Ben, I.O.; Zoiku, F.K.; Borquaye, L.S.; Gasu, E.N.; Ofori-attah, E.; Tetteh, M. Synthesis, molecular docking studies and ADME prediction of some new triazoles as potential antimalarial agents. *Sci. African* **2021**, *14*, 1–12, https://doi.org/10.1016/j.sciaf.2021.e00998.

40. Chen, J.; Si, Y.W.; Un, C.W.; Siu, S.W.I. Chemical toxicity prediction based on semi-supervised learning and graph convolutional neural network. *J. Cheminform.* **2021**, *13*, 1–16, https://doi.org/10.1186/s13321-021-00570-8.

41. Raies A.B.; Bajic, V.B. *In silico* toxicology: computational methods for the prediction of chemical toxicity. *Wiley Interdiscip. Rev. Comput. Mol. Sci.* **2016**, *6*, 147–172, https://doi.org/10.1002/wcms.1240.

42. Pang, Y.Y.; Tan, Y.M.; Chan, E.C.Y.; Ho, H.K. Phase I metabolic stability and electrophilic reactivity of 2-phenylaminophenylacetic acid derived compounds. *Chem. Res. Toxicol.* **2016**, *29*, 1118–1131, https://doi.org/10.1021/acs.chemrestox.6b00042.

43. Brenk, R.; Schipani, A.; James, D.; Krasowski, A.; Gilbert, I.H.; Frearson, J.; Wyatt, P.G. Lessons learnt from assembling screening libraries for drug discovery for neglected diseases. *Chem. Med. Chem.* **2008**, *3*, 435–444, https://doi.org/10.1002/cmdc.200700139.

44. Baell, J.B.; Holloway, G.A. New substructure filters for removal of pan assay interference compounds (PAINS) from screening libraries and for their exclusion in bioassays. *J. Med. Chem.* **2010**, *53*, 2719–2740, https://doi.org/10.1021/jm901137j.

45. Kumar, T.V.A.; Kabilan, S.; Parthasarathy, V. Screening and toxicity risk assessment of selected compounds to target cancer using QSAR and pharmacophore modelling. *Int. J. Pharm. Tech. Res.* **2017**, *10*, 219–224, https://doi.org/10.20902/ijptr.2017.10428.

46. Siddiqui, S.; Ahmed, N.; Goswami, M.; Chakrabarty, A.; Chowdhury, G. Current research in toxicology DNA damage by withanone as a potential cause of liver toxicity observed for herbal products of *Withania somnifera* (Ashwagandha). *Curr. Res. Toxicol.* **2021**, *2*, 72–81, https://doi.org/10.1016/j.crtox.2021.02.002.

47. Ito, S.; Tanaka, H.; Ojika, M.; Wakamatsu, K. Oxidative transformations of 3,4-dihydroxyphenylacetaldehyde generate potential reactive intermediates as causative agents for its neurotoxicity. *Int. J. Mol. Sci.* **2021**, *22*, 1–17, https://doi.org/10.3390/ijms222111751.

48. Indrayanto, G.; Putra, G.S.; Suhud, F. Validation of *in-vitro* bioassay methods: application in herbal drug research, 1st ed.; Elsevier Inc: Amsterdam, Netherlands, **2021**, *46*, 273-307, https://doi.org/10.1016/bs.podrm.2020.07.005.

49. Sethi, A.; Joshi, K.; Sasikala, K.; Alvala, M. Molecular docking in modern drug discovery: Principles and recent applications. *Drug Discov. Dev. - New Adv.* **2020**, *2*, 1-21, https://doi.org/10.5772/intechopen.85991.

Supplementary materials

Table S1. Ligand libraries.

Compound	Affinity energy (kcal/mol)	Molecular Weight (Da)	LogP	HA [1]	HD [2]	MR [3]	M [4]	T [5]	RE [6]	I [7]	DW [8]	Brenk	PAINS [9]	DS [10]
F1T (**Co-crystallized ligand**)	-10.12	308.3	3.47	5	1	74.08	-	-	-	-	0	0	0	-6.25
Sorgolactone (**1**)	-9.31	316.1	1.72	5	0	82.42	-	-	-	-	0	0	4	-1.36
5-Deoxystrigol (**2**)	-9.20	330.1	2.05	5	0	86.96	-	-	-	-	0	0	4	-2.89
Sorgomol (**3**)	-8.34	346.1	1.13	6	1	88.13	-	-	-	-	0	0	4	-7.94
Orobanchol (**4**)	-8.31	346.1	1.20	6	1	88.13	-	-	-	-	0	0	4	-2.51
Kukulkanin B (**5**)	-8.29	286.3	0.62	5	2	78.81	-	-	-	-	0	0	1	0.26
Hispidulin (**6**)	-8.03	300.1	-2.47	6	0	80.48	-	-	-	-	0	0	0	0.40
Demethoxyencecalin (**7**)	-7.73	202.1	2.56	2	0	60.76	-	-	-	-	0	0	0	-2.60
Demethoxyencecalinol (**8**)	-7.63	204.1	2.38	2	1	61.5	-	-	-	-	0	0	0	-3.67
Cirsiliol (**9**)	-7.60	330.1	-2.54	7	0	86.97	-	-	-	-	0	1	1	0.40
trans-Zeatin (**10**)	-7.47	219.1	-3.24	6	3	60.91	-	-	-	-	0	0	1	-0.84
Demethoxysudachitin (**11**)	-6.19	330.3	-0.96	7	1	86.97	-	++	-	-	0	0	0	0.45
Daidzein (**12**)	-8.82	254.1	0.39	4	1	71.97	-	-	++	-	0	0	0	-0.05
Jaceosidin (**13**)	-8.15	330.1	0.62	7	2	86.97	-	+	-	-	0	0	0	0.45
Lutein (**14**)	-7.98	568.4	12.00	2	2	186.76	-	-	-	-	0	0	0	0.35
1,5-Anhydro-6-deoxy-2- O-(6-deoxy-α-L-mannopyranosyl)-1-[5,7-dihydroxy-2-(4-hydroxyphenyl)-4-oxo-4H-chromen-6-yl] hexitol (**15**)	-7.87	562.2	-3.22	13	6	136.67	-	-	-	-	0	0	0	1.33
Glandulone E (**16**)	-7.78	248.0	2.85	3	1	72.24	+	-	-	-	0	1	2	-14.10
Glandulone D (**17**)	-7.75	248.3	2.38	3	0	70.57	+	+	++	-	1	1	2	-2.90
Ayapin (**18**)	-7.59	190.0	1.61	4	0	48.55	-	-	++	-	0	0	1	-3.30
7-(β-D-glucopyranosyloxy)-6-methoxycoumarin (**19**)	-7.58	354.1	-0.91	9	4	83.12	-	-	+	-	0	0	1	-5.85
Helinorbisabone (**20**)	-7.56	250.1	0.41	4	2	70.15	-	++	-	++	0	0	2	-1.14
Pectolinarigenin (**21**)	-7.53	314.1	-0.61	6	0	84.95	-	++	-	-	0	0	0	0.40
Glandulone A (**22**)	-7.52	246.3	2.67	3	0	71.28	+	-	-	++	0	1	3	-5.82
Glandulone F (**23**)	-7.47	266.3	1.79	4	2	73.92	+	-	-	-	0	1	1	-2.22
Maniladiol (**24**)	-7.45	442.4	6.49	2	2	136.04	-	-	-	-	0	0	1	-2.49
4,15-Anhydrohelivypolide (**25**)	-7.44	358.1	1.88	6	0	93.91	-	-	-	++	0	0	2	-7.51
5-O-Methylgenistein (**26**)	-7.43	284.1	1.90	5	2	78.46	-	-	++	-	0	0	0	0.04
Helibisabonol A (**27**)	-7.37	268.2	2.65	4	4	76.43	++	+	-	-	0	0	1	-2.57
Heliannone A (**28**)	-7.36	300.1	2.47	5	2	83.28	-	-	++	-	0	0	1	0.22
Gibberellin A8 (**29**)	-7.36	364.2	-2.56	7	3	88.50	-	-	-	-	0	0	1	-0.98
Helibisabonol B (**30**)	-7.35	266.2	2.40	4	4	75.96	++	+	-	-	0	0	2	0.01
Gibberellin A68 (**31**)	-7.32	346.1	-2.01	6	2	86.83	-	-	-	-	0	0	1	-1.49
Deepoxyneoxanthin (**32**)	-7.32	584.4	10.98	3	3	187.14	-	-	-	-	0	0	1	1.57
Gibberellin A4 (**33**)	-7.31	332.2	-0.88	5	1	86.14	-	-	-	-	0	0	1	-1.14
Gibberellin A1 (**34**)	-7.30	348.2	-1.71	6	2	87.34	-	-	-	-	0	0	1	-0.82
Gibberellin A75 (**35**)	-7.30	380.1	-3.41	8	4	89.66	-	-	-	-	0	0	1	-0.93
Melatonin (**36**)	-7.30	232.1	0.25	4	1	67.18	-	-	-	-	0	0	0	0.31
Silibinin (**37**)	-7.28	482.1	0.55	10	4	120.55	-	-	-	-	0	0	0	0.29
12-Oxo phytodienoic acid (**38**)	-7.27	294.2	2.66	3	0	87.55	-	-	-	-	0	0	1	-12.86
Gibberellin A72 (**39**)	-7.24	364.2	-2.56	7	3	88.50	-	-	-	-	0	0	1	-0.75
Gibberellin A29 (**40**)	-7.19	348.2	-1.71	6	2	87.34	-	-	-	-	0	0	1	-0.91
Gibberellin A20 (**41**)	-7.14	332.2	-0.86	5	1	86.18	-	-	-	-	0	0	1	-3.10
Coflotriol (**42**)	-7.10	458.4	5.73	3	3	137.21	-	-	-	-	0	0	1	-4.59
Heliannuol G (**43**)	-7.09	248.1	3.36	3	2	72.34	-	-	-	-	0	0	1	-0.37
Cyanidin 3-xyloside (**44**)	-7.06	419.1	-6.06	10	3	102.33	-	-	-	-	1	1	2	-8.74
2,3-Dihydro-2-oxo-1H-indole-3-acetic acid (**45**)	-7.05	191.1	-1.45	4	1	53.12	-	-	-	-	0	0	0	2.56
Gibberellin A67 (**46**)	-7.04	348.2	-1.71	6	2	87.34	-	-	-	-	0	0	1	-2.95
Orobanchyl acetate (**47**)	-7.04	388.2	1.06	6	1	88.16	-	-	-	++	0	0	4	-1.70

Compound	Affinity energy (kcal/mol)	Molecular Weight (Da)	LogP	HA[1]	HD[2]	MR[3]	M[4]	T[5]	RE[6]	I[7]	Unwanted Functional Group			DS[10]
											DW[8]	Brenk	PAINS[9]	
N,N′-Bis(3,4-dihydroxycinnamoyl)-1,4-butanediamine(48)	-7.02	412.2	-3.39	8	2	113.89	-	-	-	-	0	1	2	-1.57
Gibberellin A101 (49)	-7.02	362.2	-1.39	6	2	91.85	-	-	-	++	0	0	1	-2.67
Trachyloban-19-oic acid (50)	-7.01	302.2	1.69	2	0	88.42	-	-	-	-	0	0	0	-2.11
Cyanidin-3-O-glucoside (51)	-7.01	449.1	-3.51	11	6	108.29	-	-	-	-	1	1	2	-8.61
Strigyl acetate (52)	-6.99	388.2	1.69	7	0	97.86	-	-	-	-	0	0	4	-0.28
Scrophulein (53)	-6.96	314.1	2.54	6	2	84.95	-	-	-	-	0	0	0	0.40
(Z,Z)-Heliangin (54)	-6.93	362.2	2.46	6	1	95.34	-	-	-	++	1	0	0	-7.55
Gibberellin A76 (55)	-6.91	364.2	-2.56	7	3	88.50	-	-	-	-	0	0	1	-0.84
Feruloylquinic acid (56)	-6.91	368.1	-2.57	9	4	87.97	-	-	-	-	0	0	1	0.46
Gibberellin A66 (57)	-6.88	378.2	-5.59	7	1	95.02	-	-	-	-	0	0	1	-4.08
Jasmonic acid (58)	-6.87	210.1	0.21	3	0	59.18	-	-	-	-	0	0	1	-6.12
Gibberellin A44 (59)	-6.86	346.2	-0.54	5	1	90.69	-	-	-	++	0	0	1	-2.80
Rubixanthin (60)	-6.83	552.4	14.18	1	1	187.49	-	-	-	-	0	0	1	-1.85
N1,N10-Bis(p-coumaroyl)spermidine (61)	-6.83	437.2	-1.59	7	2	127.07	-	-	-	-	0	0	1	-1.93
Gibberellin A65 (62)	-6.80	362.2	-3.37	6	1	93.45	-	-	-	-	0	0	2	-7.38
Gibberellin A45 (63)	-6.79	332.2	-0.88	5	1	86.14	-	-	-	-	0	0	1	-3.53
19(10→9)-Abeo-3,4-secotirucalla-4,24-dien-3-ol (64)	-6.79	428.4	9.17	1	1	139.42	-	-	-	++	0	0	1	-10.01
Annuolide H (65)	-6.74	362.2	1.79	6	2	95.42	-	-	-	++	0	0	3	-7.50
Gibberellin A64 (66)	-6.74	346.2	-0.56	5	1	90.65	-	-	-	++	0	0	1	-3.23
Isoquercetin (67)	-6.73	464.1	-5.08	12	5	110.16	-	-	-	-	0	1	1	-3.59
23-Dehydro-25-hydroxysunpollenol (68)	-6.70	460.4	6.36	3	2	140.14	-	-	-	-	0	0	1	-6.30
Albigenic acid (69)	-6.68	472.4	3.14	4	2	137.82	-	-	-	-	0	0	1	-0.15
Heliannone C (70)	-6.68	286.3	-0.72	5	0	76.04	-	-	-	-	0	0	0	-0.08
Castasterone (71)	-6.66	464.4	3.90	5	4	132.58	-	-	-	-	0	0	0	-1.10
(2S,3S)-3,5,7-Trihydroxy-2-(4-hydroxyphenyl)-8-(3-methyl-2-buten-1-yl)-2,3-dihydro-4H-chromen-4-one (72)	-6.65	356.1	0.17	6	2	96.45	-	-	-	-	0	0	1	0.34
8-Acetoxy-1,9,14-pentadecatriene-4,6-diyn-3-ol (73)	-6.64	272.1	3.97	3	1	81.18	-	-	-	++	0	0	2	-19.98
Niveusin C (74)	-6.63	378.2	1.99	7	2	96.54	-	-	-	++	0	0	2	-8.01
Heliannuol E (75)	-6.63	248.1	3.31	3	2	72.34	-	-	-	-	0	0	1	-4.00
Sunpollenol (76)	-6.63	444.4	7.61	2	1	138.94	-	-	-	++	0	0	1	-8.48
5-Hydroxy-4,6,4'-trimethoxyaurone (77)	-6.63	328.1	2.76	6	1	87.32	-	-	-	-	0	0	1	0.20
Annuolide A (78)	-6.62	246.1	1.62	3	1	68.90	-	-	-	++	0	0	2	-8.47
Helianthoside B (79)	-6.62	1190.6	-0.92	25	14	n/a	-	-	-	-	0	n/a	n/a	-11.10
1,2-Anhydridoniveusin (80)	-6.62	376.2	1.64	7	2	96.07	-	-	-	++	0	0	3	-9.16
Heliannuol H (81)	-6.60	248.1	3.03	3	2	72.34	-	-	-	-	0	0	1	-0.81
4,5-Dihydroniveusin A (82)	-6.60	396.2	0.93	8	3	98.18	-	-	-	++	0	0	2	-11.52
3-O-Caffeoylquinic acid (83)	-6.58	354.1	-2.84	9	5	83.50	-	-	-	-	0	1	2	0.33
Brassinolide (84)	-6.57	480.3	3.22	6	4	133.67	-	-	-	-	0	0	0	-0.88
28-Norcastasterone (85)	-6.57	450.3	3.68	5	4	127.77	-	-	-	-	0	0	0	0.79
Annuolide D (86)	-6.57	248.1	1.80	3	1	69.38	-	-	-	-	0	0	1	-2.27
Indole-3-acetaldehyde (87)	-6.57	159.1	1.32	2	1	48.27	-	-	-	++	0	0	1	-2.18
ent-Kaur-16-en-19-oic acid (88)	-6.55	302.2	2.04	2	0	90.32	-	-	-	-	0	0	1	-4.80
ent-Kaurene (89)	-6.53	272.3	5.39	0	0	88.54	-	-	-	-	0	0	1	-7.85
Heliannuol J (90)	-6.52	264.1	0.50	4	1	71.67	+	-	-	-	1	0	1	-0.45
N,N′-1,4-Butanediylbis[3-(4-hydroxyphenyl)-2-propenamide] (91)	-6.52	380.2	-2.70	6	0	109.84	-	-	-	-	0	0	1	-1.62
Schottenol (92)	-6.50	414.4	7.86	1	1	133.23	-	+	-	-	0	0	1	-4.48

Compound	Affinity energy (kcal/mol)	Molecular Weight (Da)	LogP	HA [1]	HD [2]	MR [3]	M [4]	T [5]	RE [6]	I [7]	Unwanted Functional Group			DS [10]
											DW [8]	Brenk	PAINS [9]	
Indole-3-ethanol (**93**)	-6.49	161.1	1.53	2	2	49.23	++	-	-	-	0	0	0	-1.98
Annuolide F (**94**)	-6.46	344.2	2.59	5	1	93.75	-	-	-	++	0	0	3	-8.92
Heliannuol I (**95**)	-6.45	264.1	0.50	4	1	71.67	+	-	-	-	1	0	1	-0.45
Sudachitin (**96**)	-6.45	358.3	-1.03	8	1	93.47	++	++	-	-	0	0	0	0.45
Gibberellin A100 (**97**)	-6.45	364.2	-3.06	6	2	94.45	-	-	-	-	0	0	1	-3.45
Helikauranoside A (**98**)	-6.44	482.3	1.38	8	5	123.93	-	-	-	-	0	0	0	-8.59
Gibberellin A19 (**99**)	-6.43	362.2	-3.35	6	1	93.49	-	-	-	-	0	0	2	-6.91
Peposterol (**100**)	-6.42	412.4	8.38	1	1	132.75	-	+	+	+	0	0	1	0.41
Tanegool (**101**)	-6.37	376.2	1.21	7	4	98.25	-	-	-	-	0	0	0	-0.55
Helivypolide D (**102**)	-6.35	360.2	2.57	6	1	94.91	-	-	-	++	0	0	0	-8.67
Tricin 5-O-β-D-glucoside (**103**)	-6.32	492.1	-1.37	12	5	119.10	-	-	-	-	0	0	0	-3.00
Heliannone B (**104**)	-6.30	300.1	1.13	5	0	80.51	-	-	-	-	0	0	0	-0.08
Heliannuol F (**105**)	-6.29	264.1	2.68	4	2	73.02	-	-	-	-	0	0	0	0.17
15-Hydroxyleptocarpin (**106**)	-6.28	378.2	1.53	7	2	96.51	-	-	-	++	1	0	4	-7.87
Neochlorogenic acid (**107**)	-6.27	354.1	-6.00	9	3	83.50	-	-	-	-	0	1	2	0.33
Costunolide (**108**)	-6.27	232.1	4.18	2	0	69.85	-	-	-	++	0	0	2	-9.16
Tambulin (**109**)	-6.25	344.1	0.74	7	1	91.44	-	++	++	-	0	0	0	0.11
(-)-Loliolide (**110**)	-6.22	196.1	0.91	3	1	52.51	-	-	-	-	0	0	0	-4.22
Helivypolide E (**111**)	-6.19	376.2	1.49	7	1	95.54	-	-	-	++	1	0	3	-7.14
1-Benzoyl-2-nonadecanone (112)	-6.18	386.3	8.66	2	0	123.36	-	-	-	-	0	0	1	-28.49
Gibberellin A102 (**113**)	-6.17	378.2	-4.20	7	2	94.65	-	-	-	-	0	0	2	-6.75
5-Deoxynevadensin (**114**)	-6.14	328.1	2.82	6	1	89.42	-	++	-	-	0	0	0	0.40
Gibberellin A12 (**115**)	-6.14	332.2	-1.38	4	0	92.09	-	-	-	-	0	0	1	-4.49
Heliannuol C (**116**)	-6.06	248.1	3.29	3	2	72.34	-	-	-	-	0	0	1	-4.44
Heliannuol A (**117**)	-6.06	250.2	3.29	3	2	72.82	-	-	-	-	0	0	0	-2.39
Sucrose-6-phosphate (**118**)	-6.04	422.1	-9.10	14	8	79.07	-	-	++	-	0	0	1	-30.84
Xanthomicrol (**119**)	-5.99	344.3	0.89	7	1	91.44	-	++	-	-	0	0	0	0.45
Helianthoside A (**120**)	-5.99	1058.6	-1.76	21	11	n/a	-	-	-	-	0	n/a	n/a	-6.45
Skullcapflavone II (**121**)	-5.99	374.1	2.40	8	2	97.93	++	++	-	-	0	0	0	0.40
Heliannuol K (**122**)	-5.98	248.1	3.25	3	1	71.85	-	-	-	-	0	0	0	-3.83
Acerosin (**123**)	-5.93	360.3	-1.03	8	1	93.47	++	++	-	-	0	0	0	0.45
Heliannuol L (**124**)	-5.87	266.2	2.26	4	3	73.98	-	-	-	-	0	0	0	-0.99
Hymenoxin (**125**)	-5.85	374.3	0.82	8	1	97.93	++	++	-	-	0	0	0	0.45
Sideritiflavone (**126**)	-5.84	360.3	0.55	8	2	93.47	++	++	-	-	0	1	1	0.45
Helianthoside 5 (**127**)	-5.81	1220.6	-1.52	26	15	n/a	-	-	-	-	0	n/a	n/a	-5.00
Methoxysudachitin (**128**)	-5.78	374.3	0.82	8	1	n/a	-	++	-	-	0	n/a	n/a	0.45
Annuionone H (**129**)	-5.78	282.2	1.74	4	2	77.71	-	-	-	-	0	0	1	3.11
N-(4-Amino-1-carboxybutyl)glutamic acid (**130**)	-5.67	262.1	-8.43	8	2	61.01	-	-	-	-	0	0	0	0.39
Helianyl octanoate (**131**)	-5.63	554.5	12.38	2	0	178.00	-	-	-	++	0	0	1	-32.37
Heliannuol D (**132**)	-5.62	250.2	3.38	3	2	72.82	-	-	-	-	0	0	0	-2.02
Annuionone C (**133**)	-5.60	224.1	1.48	3	1	62.17	-	-	-	++	1	0	2	-0.93
Annuionone E (**134**)	-5.55	226.2	1.72	3	1	62.60	-	-	-	++	0	0	0	-4.70
Annuionone G (**135**)	-5.44	226.2	1.31	3	3	63.99	-	-	-	++	0	0	0	-0.41
Annuionone B (**136**)	-5.43	222.1	1.44	3	0	61.17	-	++	-	++	0	0	1	-0.93
2,3,4-Trimethylhexane (**137**)	-5.35	128.2	3.45	0	0	45.38	-	-	-	-	0	0	0	-4.20
5,6-Epoxy-9-hydroxy-7-megastigmen-3-one (**138**)	-5.29	226.2	1.75	3	2	64.32	-	-	-	++	0	0	1	-1.93
Sundiversifolide (**139**)	-5.29	224.1	1.54	3	1	62.35	-	-	-	-	0	0	1	-0.11
Sucrose (**140**)	-5.26	342.1	-4.61	11	8	68.16	-	-	++	-	0	0	0	-6.85
(+)-Loliolide (**141**)	-5.25	196.1	0.91	3	1	52.51	-	-	-	-	0	0	0	-4.22
8,10-Nonacosanedione (**142**)	-5.23	436.4	11.14	2	0	141.92	-	-	-	-	0	0	1	-28.66
(+)-Dehydrovomifoliol (**143**)	-5.21	222.1	1.61	3	1	62.88	-	++	-	++	0	0	1	-3.61
Annuionone A (**144**)	-5.15	224.1	1.69	3	0	61.64	-	-	-	++	0	0	0	-1.61
Quinic acid (**145**)	-5.09	192.1	-4.41	6	4	40.11	-	-	-	-	0	0	0	1.85
Annuionone F (**146**)	-5.06	242.2	0.82	4	3	65.48	-	-	-	++	0	0	1	-6.96

Compound	Affinity energy (kcal/mol)	Molecular Weight (Da)	LogP	HA [1]	HD [2]	MR [3]	M [4]	T [5]	RE [6]	I [7]	Unwanted Functional Group			DS [10]
											DW [8]	Brenk	PAINS [9]	
12,14-Nonacosanedione (147)	-5.01	436.4	11.14	2	0	141.92	-	-	-	-	0	0	1	-28.49
Caprolactam (148)	-4.84	113.1	0.52	2	1	35.76	++	++	++	++	0	0	0	-7.96
Fumaric acid (149)	-4.79	116.0	-5.07	4	0	24.41	-	-	-	-	0	0	1	-0.47
12,14-Tritriacontanedione (150)	-4.76	492.5	12.96	2	0	161.15	-	-	-	-	0	0	1	-28.49
Helianthoside 2 (151)	-4.70	1352.7	-2.75	30	17	n/a	-	-	-	-	0	n/a	n/a	-10.78
Helianthoside 4 (152)	-4.22	1368.7	-3.68	31	18	n/a	-	-	-	-	0	n/a	n/a	-14.32
Isoprene (153)	-3.79	68.1	2.12	0	0	25.2	++	++	+	+	0	0	1	-13.02
Helianthoside 1 (154)	-3.52	1336.7	-1.90	29	16	n/a	-	-	-	-	0	n/a	n/a	-11.08
Helianthoside 3 (155)	-1.33	1382.7	-3.36	31	18	n/a	-	-	-	-	0	n/a	n/a	-10.78

[1] Hydrogen Acceptor; [2] Hydrogen Donor; [3] Molar Refractivity; [4] Mutagenic; [5] Tumorigenic; [6] Reproductive Effects; [7] Irritant; [8] DataWarrior; [9] Pan Assay Interference Compounds; [10] Druglikeness Score
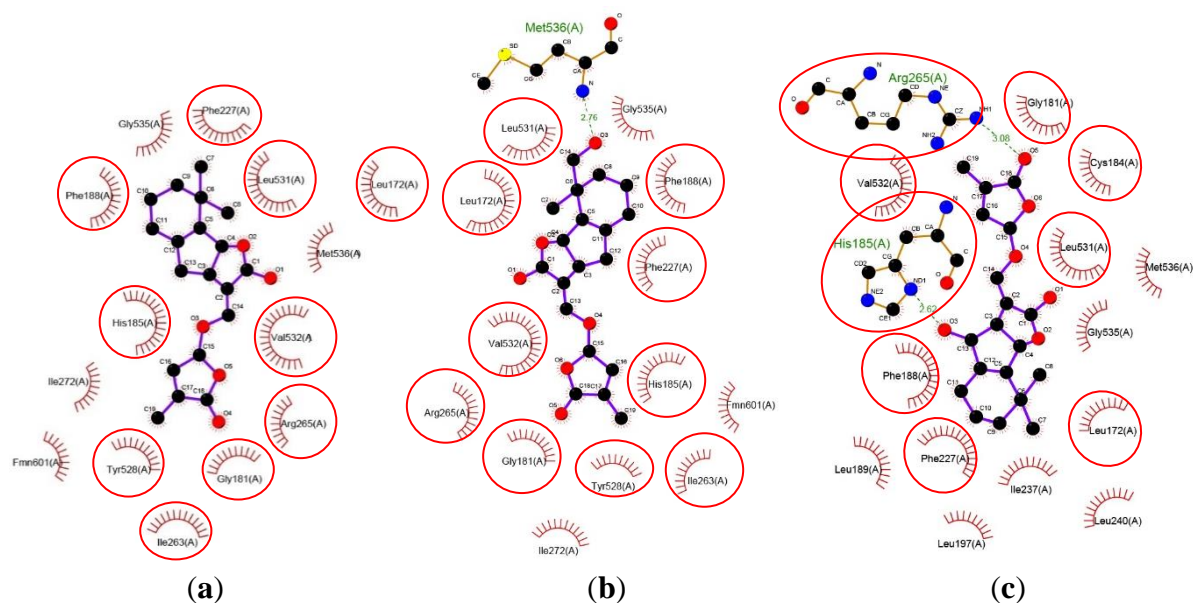

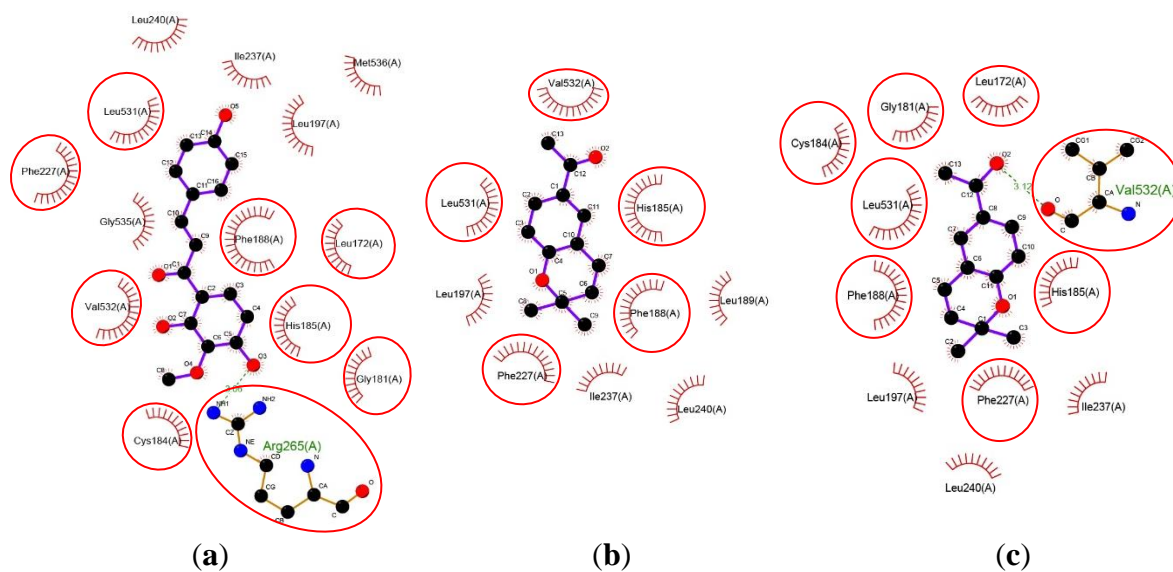**Figure S1**. Interaction of 5-deoxystrigol (**a**), sorgomol (**b**), orobanchol (**c**) ligands with *Pf*DHODH residues

Figure S2. Interaction of kukulkanin B (**a**), demethoxyencecalin (**b**), demethoxyencecalinol (**c**) ligands with *Pf*DHODH residues

(**a**)   (**b**)   (**c**)
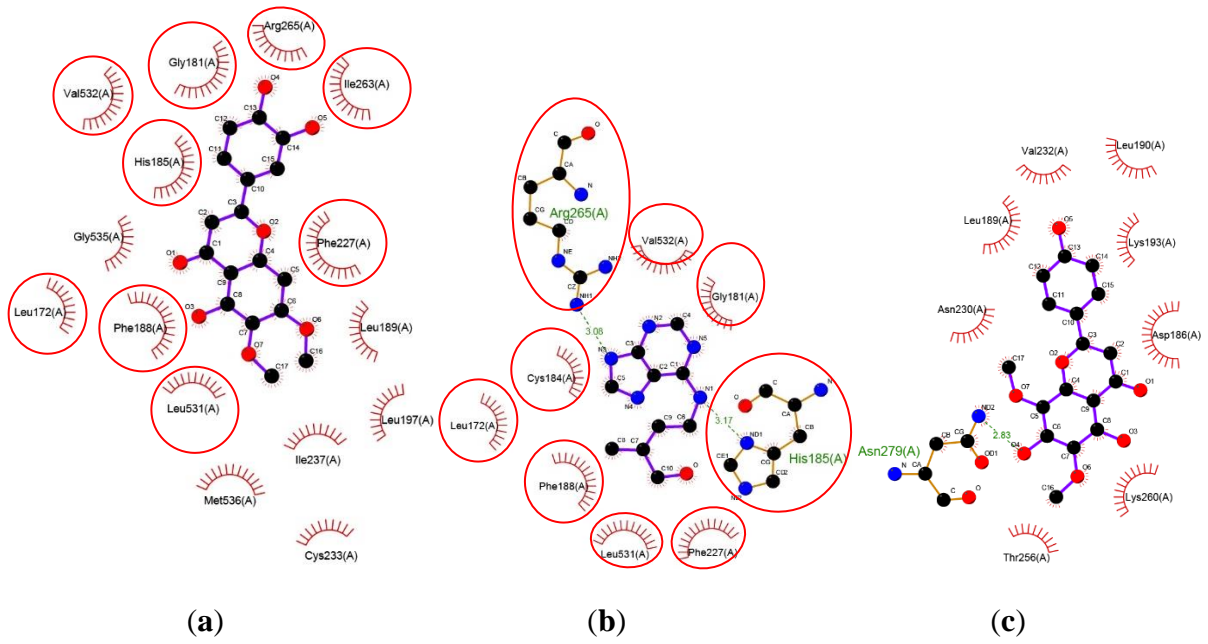
Figure S3. Interaction of cirsiliol (**a**), *trans*-zeatin (**b**), demethoxysudachitin (**c**) ligands with *Pf*DHODH residues.